Juniper Online
Journal Material Science
ISSN: 2575-856X

Research Article
Volume 10 Issue 4 - May 2026
DOI: 10.19080/JOJMS.2026.10.555792

JOJ Material Sci

Room-Temperature Methane Gas Sensing with Carbonization of Poly (Vinyl) Alcohol/Tin Dioxide/Graphene Oxide Nanofiber by Electrospinning

Chan Wing-Yu and Lam King-Cheong*

Division of Science, Engineering and Health Studies, School of Professional Education and Executive Development, The Hong Kong Polytechnic University, Hong Kong, China

Submitted: April 26, 2026; **Published:** May 11, 2026

***Corresponding author:** Lam King-Cheong, Division of Science, Engineering and Health Studies, School of Professional Education and Executive Development, The Hong Kong Polytechnic University, Hong Kong, China

Abstract

This study reports on the characteristics of room-temperature methane sensing due to the carbonization of composite nanofibers synthesized from poly(vinyl) alcohol/tin dioxide/graphene oxide using an electrospinning technique. It is noted that the addition of graphene oxide leads to the formation of porous structure in the composite nanofiber, which significantly improves methane detection efficiency. Porosity in the nanofiber is assumed to improve the gas-solid interaction by strengthening the p–n junction in a composite nanofiber made from a p-type poly(vinyl) alcohol/graphene oxide and an n-type tin dioxide, and at the same time, minimizing the shielding effect caused by amorphous carbon on the surface in the core–shell type nanofiber. Carbonization not only improves the methane detection efficiency by lowering the resistance but also maintains sensitivity at room temperature. When the graphene oxide in poly(vinyl) alcohol is 8wt%, the highest sensitivity towards 1% methane is measured to be 60.5% at a carbonization temperature of 550°C.

Keywords: Methane gas sensor; Electro spun composite nanofibers; Graphene oxide; Tin dioxide; Room-temperature gas sensing

Abbreviations: CNTS: Carbon Nanotubes; RGO: Reduced Graphene Oxide; GO: Graphene Oxide; SEM: Scanning Electron Microscope; TEM: Transmission Electron Microscope; FTIR: Fourier Transform Infrared Spectroscopy; TGA: Thermogravimetric Analysis; DTG: Differential Thermogravimetric Analysis; PVA: Poly (Vinyl Alcohol)

Introduction

Recently, the applications of one-dimensional metal oxide nanofibers in gas sensors have received attention since these materials have high surface area and porosity which effectively convert gas-solid reactions into electrical responses due to directional charge transport [1-6]. Tin dioxide (SnO_2), as a non-toxic, economical, widely accessible n-type wide-band gap semiconductor material (Eg = 3.6eV) has been proven sensitive to numerous gases due to oxygen vacancies on the surfaces of SnO_2 generated by annealing as active sites in gas-solid reactions [7-13]. Therefore, sensors based on SnO_2 nanofibers are believed to be effective gas sensing materials [4-6,14-22]. However, they usually work at relatively high temperatures which limits their usage in miniaturized electronic devices [4-6,14,18,20]. Very limited studies have been done to develop SnO_2 nanofiber heterostructures in order to reduce operating temperatures [15,16,17,19,21,22]. For instance, [21] have reported the fabrication of Pt-SnO_2/RGO nanocomposites using a microwave-assisted method and investigated hydrogen sensing performance at temperatures as low as 50°C. [15] have reported SnO_2 nanofibers containing reduced graphene oxide (RGO) synthesized via electrospinning and analyzed gases at an operating temperature of 50°C. But, room-temperature working capability has not been extensively studied yet. For example, [19] have developed SnO_2 nanofibers containing carbon nanotubes (CNTs) via electrospinning and explored carbon monoxide sensing. Moreover, [16] have developed PAN/PVP/SnO_2/ZnO nanofibers followed by carbonization process and explored DMMP gas sensing. Therefore, there is still a great deal of work needed to be done in order to develop SnO_2 nanofiber gas sensors which can work at relatively low temperatures.

Recently, the unique properties of graphene, such as excellent mechanical and electrical properties, which derive from its 2-D structure consisting of few-layer sp^2 hybridization of carbon atoms, have attracted a lot of interest for various uses including sensing and electronics applications [23-27]. Recently, graphene derivatives, particularly graphene oxide (GO), have become popular in sensors, batteries, and biomedicine applications due to functional groups, especially oxygen-containing ones. The GO material is made of few-layer graphite oxide generated through chemical oxidation and subsequent exfoliation processes [28-30]. Oxygen-containing functional groups including hydroxyl, epoxy, carbonyl, and carboxyl groups on the basal plane or edge of the sheets act as active sites in gas-solid reactions in sensors. GO/SnO_2 nanofibers can improve the sensing performances based on p-n junction effect [31,32]. However, the oxygen functional groups tend to attract electrons which results in the surface formation of space-charge layer which reduces the electrically conductivity of GO materials [33]. Reduction of GO materials into reduced graphene oxide (RGO) by chemical or thermal reduction process removes the oxygen functional groups. Chemically, [34] reported hydrazine-mediated reduction of GO for the first time in the literature. The highest conductivity reported in hydrazine-mediated reduction is 99.6Scm^{-1} with a C/O ratio of 12.5 [35]. On the other hand, [35] chemically reduced GO using vitamin C. With the C/O ratio of 12.5, 77 S cm^{-1} was achieved in this work. Thermally, [36] found that the C/O ratio of GO increases from 2.6/1 at room temperature to 9.7/1 at 1050°C suggesting removal of oxygen functional groups at high temperatures. [37] annealed GO sheets at 500°C, 700°C, and 1100°C under Ar/H_2 and achieved conductivity of 49, 93, and 550Scm^{-1}, respectively. As it can be seen, the higher the temperature, the higher the conductivity of GO. Although, RGO has superior conductivity compared to GO, it has relatively low p-type character due to some residual oxygen-containing groups after thermal reduction. Hybridization of RGO with some metal oxides like SnO_2 significantly improves gas sensing properties at much lower operating temperatures due to high conductivity of RGO [15,38,39].

The methane gas is non-toxic, colorless, and odorless and the main component in natural and fuel gases. Methane is highly flammable and even slight leaks might lead to explosions, which has been proved with some pipeline accidents [40-46]. The lower explosion limit of methane in air is about 4.7% [47]. Currently, methane sensors reported use semiconducting metal oxides and operate at relatively high temperatures, ranging from 150 to 350°C [48-52]. Therefore, current researches aim to develop methane sensors which can operate at lower temperatures.

Among various polymers used for electrospinning, PVA polymer is widely used due to its rich hydroxyl groups on the chains which facilitate bonding between PVA and GO to improve thermal and mechanical properties of composites which suitable for the applications in material filler, barrier film and biomedical engineering [53-56]. This work aims to synthesize PVA/SnO_2/GO nanofibers by one-step electrospinning method and subsequent carbonization under nitrogen atmosphere for enhanced electrical conductivity and high room-temperature sensing performance. After carbonization, both PVA and GO pyrolyze to generate carbon nanofibers with some residual oxygen groups. The improved thermal stability due to the bond formation of oxygen groups enhances the yield of carbon nanofibers after carbonization. The proposed method offers simple and low-cost way of preparing carbon nanofibers compared to most electro spun PAN-based carbon nanofibers [57-60]. The present work investigated the structural morphology, thermal behavior, crystallinity, functional groups, electrical resistance, and gas sensing performances of the composite nanofibers.

Materials and Methods

Materials

Graphite powder (1000 mesh) was purchased from QingDao HuaTai Lubricant Sealing S&T Co. Ltd. The dihydrate form of stannous chloride and polyvinyl alcohol (PVA, average molecular weight ≈ 105,000) were purchased from Xilong Scientific Co., Ltd. Potassium permanganate was provided by Tianjin Kermal Chemical Reagent Co., Ltd. Sodium nitrate was obtained from Tianjin ZhiYuan Chemical Reagent Co. Ltd. Sulfuric acid (95%) was purchased from Sigma Aldrich. Hydrogen peroxide (35%) and hydrochloric acid (1N) were purchased from VWR International Ltd.

Preparation of GO

The production of GO was achieved by modifying the Hummers process [61]. In essence, concentrated sulfuric acid (25mL; 95%) was first added to a beaker comprising graphite flakes (1.0g; 1000 mesh) and sodium nitrate (1.25g). Then, the mixture was stirred vigorously for 1h. Potassium permanganate (3.7g) was progressively added to the suspension, which was stirred vigorously for 3h at 35°C. During the process, gases were evolved while the suspension turned into a brown paste-like material. Afterwards, icy water (150mL) was slowly added to the brown paste, whereby the temperature increased to about 90°C. Gas evolution stopped when the stirring ended. Following that, hydrogen peroxide (30 mL; 35%) was added to the paste, which turned into a bright yellow paste. The latter was filtered and washed with deionized water (40mL) and 1N hydrochloric acid (20mL) three times.

Preparation of PVA/ SnO_2/GO nanofiber

The electrospinning precursor solution was made using PVA (5wt%, Mw ≈ 105,000) together with $SnCl_2{\cdot}2H_2O$ powder and GO suspension. First, PVA powder (2g) was mixed with distilled water (40mL) and vigorously stirred at 95°C for 2h. Subsequently, SnCl2·2H2O powder (4g) was dissolved in the polymer solution and vigorously stirred at 95°C for 15min. A number of GO suspensions were made using various amounts of GO (0.02g, 0.04g, 0.08g and 0.16g). The GO powder was ground into smaller particles before being dispersed into distilled water (15mL).

How to cite this article: Chan W.Y., Lam K.C. Room-Temperature Methane Gas Sensing with Carbonization of Poly (Vinyl) Alcohol/Tin Dioxide/Graphene Oxide Nanofiber by Electrospinning. JOJ Material Sci. 2026; 10(4): 555792. DOI: 10.19080/JOJMS.2026.10.555792

Vigorous stirring and sonication were then carried out on the mixture for 2h each. The resultant GO suspension was blended into the preformed PVA/$SnCl_2$·$2H_2O$ solution and vigorously stirred at 95°C for 15min. The electrospinning precursor solution of PVA/$SnCl_2$·$2H_2O$/GO was fabricated into composite nanofibers using the roller electrospinning technique at a voltage of 75kV and a collector-roller gap of 190mm. The resultant nanofibers were collected upwardly on the surface of glass substrates fixed on aluminum foil attached to the grounded electrode. The as-spun composite nanofibers with various GO contents were immediately transferred to a desiccator for carbonization under nitrogen gas at 400, 450, 500, 550, 600, and 650°C for 1h at a heating rate of 10°C/min. The carbonization process led to the color transition of the nanofibers from white to brown to black. The fibers were designated based on the amount of GO relative to the PVA in the precursor solutions as 0wt%, 1wt%, 2wt%, 4wt%, and 8wt%. For sensor fabrication, gold electrodes (2 × 10mm) with a 5mm inter-electrode spacing were coated onto the composite nanofibers surface.

Results and Discussion

Morphology analyses were carried out using a Scanning Electron Microscope (SEM) with a voltage of 200 kV (JEOL Model JSM-6490), while transmission electron microscopy was done with a Transmission Electron Microscope (TEM) (JEOL Model JEM-2011). For thermal properties, the Thermogravimetric Analyzer/Differential Scanning Calorimeter (TGA/DSC) (Netzsch STA 449C, Jupiter) was used. The Raman spectra were measured using a Horiba Lab RAM HR 800 spectrometer. For crystal structure analysis, the X-ray diffraction method (Rigaku smart Lab, 9kW rotating anode, Cu Kα, λ = 1.542Å) was applied. Fourier Transform Infrared Spectroscopy (FTIR) analysis was executed using a Bruker Vertex-70 FTIR spectrophotometer. The sensor tests were carried out in an assembly gas cell fitted with mass flow controllers (KellHua), whereas electrical characterization was done using a Keithley 2400 sourcemeter.

SEM analysis

Successful synthesis of PVA/SnO_2/GO nanofibers with different contents of GO was confirmed from SEM micrographs shown in Figure 1a-1f. These nanofibers possessed uniform and smooth morphologies with decreased fiber diameters as the amount of GO was increased. Figure 2a-2f demonstrates the diameters of nanofibers as histograms for PVA/SnO_2/GO nanofibers with mean diameters of 293,267,233,248,189 and 151nm for different amounts of GO, calculated by measuring 100 fibers randomly selected. Comparison between these diameters shows that the composite nanofibers possess small fiber diameters for high GO content. It is considered that enhanced conductivity caused by the increase of GO content leads to decreased fiber diameters. There are three controlling factors for nanofiber morphology: (1) surface tension, (2) conductivity, and (3) viscosity [40,62-65]. As surface tension tries to reduce surface area of jet as much as possible by changing straight jet to sphere drops, whereas conductivity, depending on charge density, elongates jet due to electrostatic repulsion force among charged ions leading to decrease in fiber diameters. The rapid distortion of the fiber shape is controlled by viscosity.

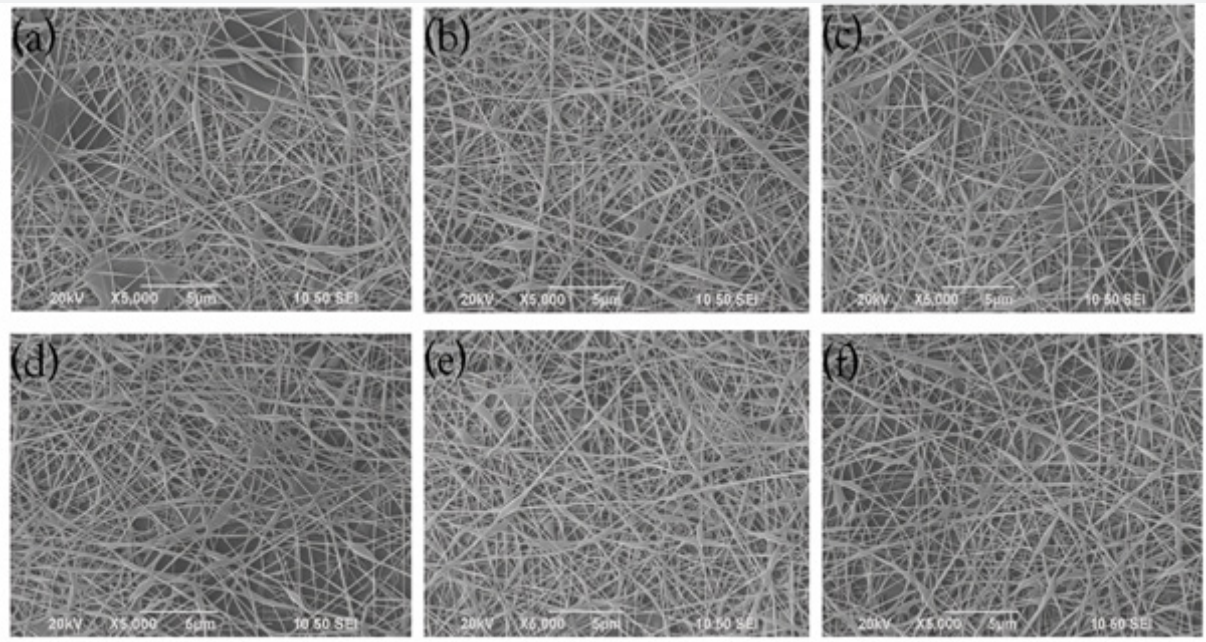

Figure 1: SEM images of (a) 0 wt%, (b) 1 wt%, (c) 2 wt%, (d) 2 wt% (before carbonization), (e) 4 wt% and (f) 8 wt%.

How to cite this article: Chan W.Y., Lam K.C. Room-Temperature Methane Gas Sensing with Carbonization of Poly (Vinyl) Alcohol/Tin Dioxide/Graphene Oxide Nanofiber by Electrospinning. JOJ Material Sci. 2026; 10(4): 555792. DOI: 10.19080/JOJMS.2026.10.555792

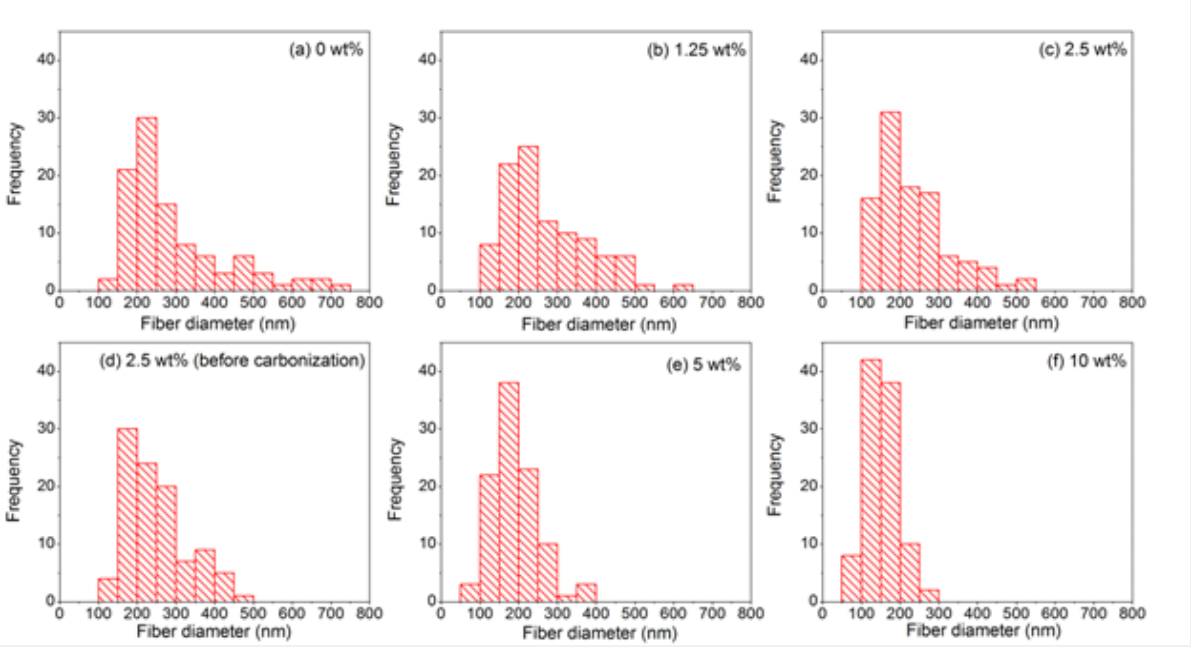

Figure 2: Fiber diameter distributions of (a) 0 wt%, (b) 1 wt%, (c) 2 wt%, (d) 2 wt% (before carbonization), (e) 4 wt% and (f) 8 wt%.

The introduction of GO into the polymer composite will increase the electrical conductivity and viscosity of the polymer composite, thus helping the formation of smooth, non-beaded nanofibers. However, from the observation of narrower fibers at higher levels of GO, the effect of electrical conductivity becomes more significant than that of viscosity. The acceleration stage of jet movement towards the collector involves electrostatic repulsion between the particles along the axis of the jet stream and evaporation of the solvent in the jet stream, thus causing thinning of the jet stream. Higher viscosity will inhibit the process of stretching the jet stream by increasing its inertia; hence, it causes increased fiber thickness. On the other hand, increased electrical conductivity results in higher charge density; thus, electrostatic repulsion enhances jet stretching, resulting in reduced fiber thickness.

TEM analysis

Selected transmission electron microscopy (TEM) micrographs of samples doped with 0wt%, 4wt%, and 8wt% GO after carbonization at 550°C in N_2, as depicted in Figure 3a-3c, show homogeneous size and morphology of nanofibers with agglomerated SnO_2 nano crystallites uniformly deposited onto their surfaces. The nanofiber diameter appears to be the smallest for samples with 8 wt% GO, as can be observed in Figure 3c, in good agreement with the results obtained in SEM analysis and higher amounts of GO content. The sample with no GO doping exhibits a core–shell morphology (Figure 3a), and a notable difference in contrast is observed between the core and shell sections. In this scenario, SnO_2 nano crystallites uniformly cover the nanofiber shell and encapsulate the PVA core. The formation of the core–shell morphology is caused by the separation of the phases during electrospinning and the Kirkendall effect during carbonization [66-68]. Due to the high surface tension, PVA tends to accumulate in the core, while the movement of the Sn precursor is facilitated by the diffusion towards the surface of the fiber, which is caused by solvent evaporation during electrospinning. In the course of carbonization, the Sn precursor diffuses further towards the nanofiber surface, which results from the formation of SnO_2 on the fiber surface.

Porosity and void areas are present on the surface of the 4wt% and 8wt% samples containing GO Figure 3b & 3c. The porous morphology of the nanofiber structures for these samples is achieved after adding GO because of the immobilization effect of PVA and Sn precursors through cross-linking between GO and PVA in the electrospinning and carbonization process. The immobilizing influence of GO addition has already been reported in other studies [69-72]. Selected high-resolution TEM (HRTEM) micrographs of samples containing 0 wt%, 4 wt%, and 8 wt% GO are shown in Figures 3d-3f. Interspaces equal to ~0.35nm and ~0.26nm belong to (110) and (101) planes of rutile SnO_2, respectively. In Figure 3d, the marked section consists of amorphous carbon formed due to the carbonization of PVA located inside the core. Particles of amorphous carbon diffuse outwards and form a thin layer of amorphous carbon outside the SnO_2 shell after carbonization. An increase in the amount of GO leads to the decrease in the amount of amorphous carbon, as seen in Figures 3e & 3f; thus, samples with 4wt% and 8wt% contain more porous structures and consequently lead to the degradation of PVA and GO into volatile organic compounds due to less shielding as compared to the core–shell structure of the 0wt% sample.

How to cite this article: How to cite this article: Chan W.Y., Lam K.C. Room-Temperature Methane Gas Sensing with Carbonization of Poly (Vinyl) Alcohol/Tin Dioxide/Graphene Oxide Nanofiber by Electrospinning. JOJ Material Sci. 2026; 10(4): 555792. DOI: 10.19080/JOJMS.2026.10.555792

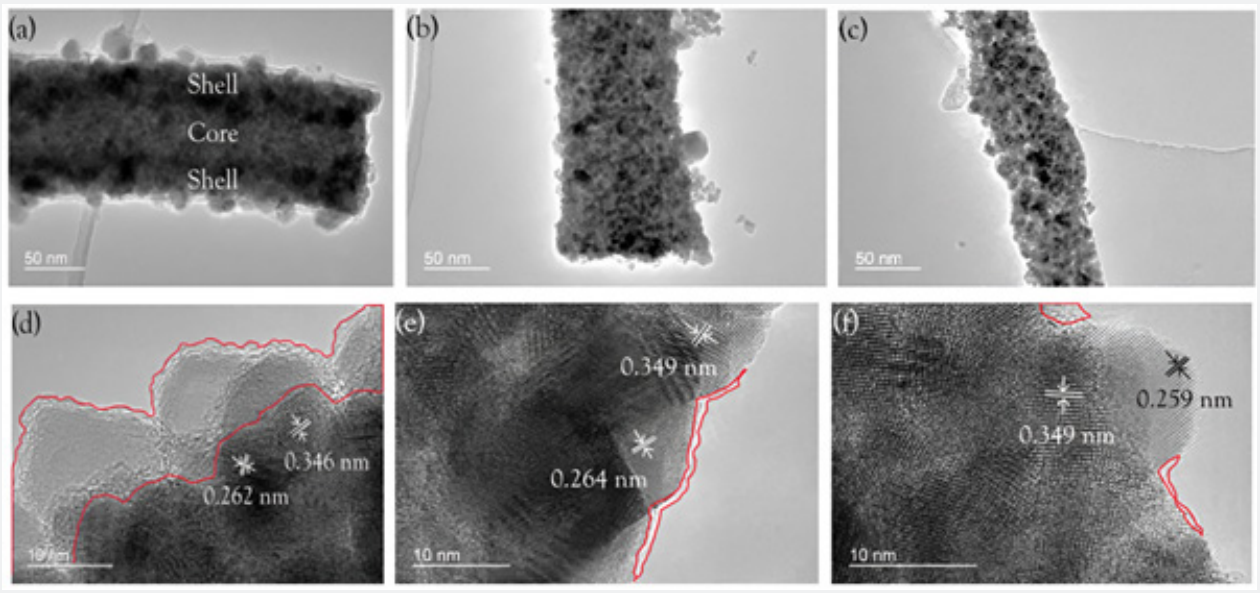

Figure 3: Representative TEM images of (a) 0 wt%, (b) 4 wt% and (c) 8 wt%. HRTEM images of (d) 0 wt%, (e) 4 wt% and (f) 8 wt%.

TGA analysis

In order to investigate the thermal stability of the composite nanofibers of different GO concentrations (0, 1,2,4, and 8wt%), thermogravimetric analysis (TGA) and differential thermogravimetric analysis (DTG) were conducted under nitrogen conditions, as illustrated in Figures 4a & 4b. All of the composite nanofibers exhibited three significant weight losses (Figure 4a). The initial weight loss at approximately 179–226 °C can be ascribed to the oxidation of labile oxygen-containing functional groups from PVA and GO materials, leading to the release of H_2O or O_2. It should be noted that the amount of the first-stage weight loss in the samples increases in the order of 0,1,2,4, and 8wt%, as depicted in Figure 4a. This is probably attributed to the increased thermal stability associated with the cross-linking reaction between GO and PVA [53-56]. In comparison with the onset temperature of the first weight loss of the 0wt% sample (194 °C) illustrated in Figure 4b, the onset temperatures of 1 and 2wt% samples are relatively higher at 226°C and 221°C, respectively, which can be explained by possible cross-linking effects between GO and PVA. On the other hand, the onset temperatures of the 4 and 8wt% samples are relatively lower at 183°C and 179°C, respectively, which may be attributed to the removal of oxygen-containing functional groups from GO, not participating in the cross-linking reaction. The second weight loss of the 0wt% sample occurred at 331°C and is related to the oxidation of residual oxygen-containing functional groups of PVA and GO as well as the PVA side chains. The third weight loss for the 0wt% sample at 438°C can be attributed to the oxidation of the carbon backbones of PVA and GO. As for the 1wt% to 8wt% samples, the second and third weight losses took place approximately at 410°C and 455°C, respectively, which were relatively higher in value when compared with those values of 0 wt%, according to previous studies [53,73,74-76]. Furthermore, it can be seen that the second weight loss of the 1–8wt% samples was more significant than that of the third one, suggesting that the effect of the cross-linking interaction between PVA and GO on the oxygen-containing side chain was larger than on the carbon backbone.

Raman analysis

The Raman spectra of the composite nanofibers both before and after carbonization are shown in Figure 5a & 5b respectively. In Figure 5a, the peak at 2917cm^{-1} found in 0wt% composite nanofibers is assigned to the C-H stretching vibration of poly (vinyl alcohol) (PVA). The absence of the peak in all composite nanofibers containing graphene oxide (GO) from 1wt% to 8wt% can be due to surface modification of the nanofibers with GO, similar to previous studies [77]. The G band in all composite nanofibers appears after GO addition around 1590cm^{-1}. The wide band at 3060cm^{-1} for 8 wt% composite nanofibers relates to the stretching vibration of =C-H bonds of GO. A weak peak in all composite nanofibers at 610cm^{-1} is associated with Sn-O vibrations. The D and G bands show up around 1360cm^{-1} and 1590cm^{-1}, respectively, after carbonization in Figure 5b. The D band is related to defects of sp^3 carbon vibrations, while the G band is correlated to sp^2 carbon vibrations of pristine graphitic structures [78,79]. The intensities of the G bands in Figure 5b are relatively higher than those in Figure 5a since graphitic domains have increased due to the addition of amorphous carbon resulting from the carbonization process of PVA and GO. The value of the ID/IG ratio decreases from 0.754 to 0.636 when GO contents increase from 0wt% to 8wt%. The D band intensity reduces while the G band intensity increases with increasing GO contents from 0wt% to 8wt%.

How to cite this article: Chan W.Y., Lam K.C. Room-Temperature Methane Gas Sensing with Carbonization of Poly (Vinyl) Alcohol/Tin Dioxide/Graphene Oxide Nanofiber by Electrospinning. JOJ Material Sci. 2026; 10(4): 555792. DOI: 10.19080/JOJMS.2026.10.555792

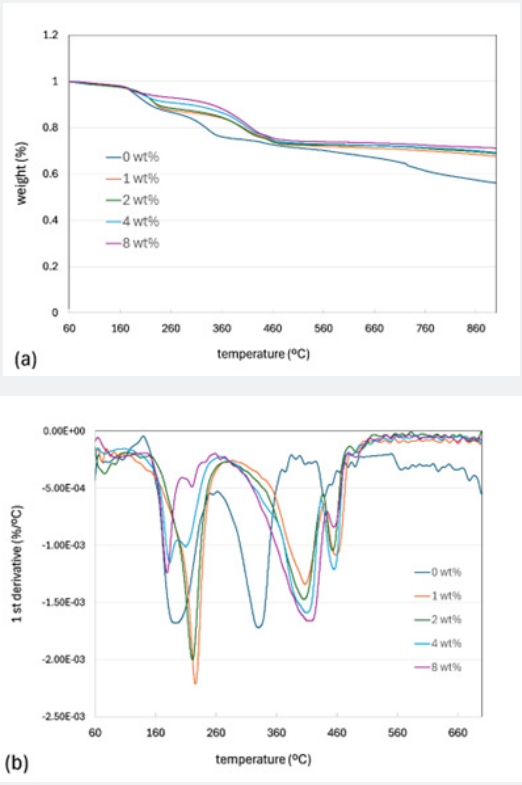

Figure 4: (a) TGA and (b) DTG spectra of the composite nanofibers.

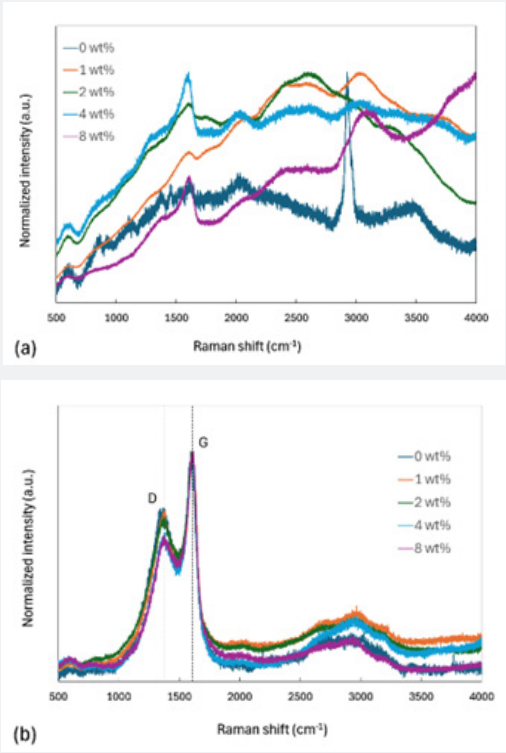

Figure 5: Raman spectra of the composite nanofibers of PVA/SnO_2/GO with different GO contents (a) before carbonization and (b) after carbonization.

How to cite this article: How to cite this article: Chan W.Y., Lam K.C. Room-Temperature Methane Gas Sensing with Carbonization of Poly (Vinyl) Alcohol/Tin Dioxide/Graphene Oxide Nanofiber by Electrospinning. JOJ Material Sci. 2026; 10(4): 555792. DOI: 10.19080/JOJMS.2026.10.555792

XRD analysis

X-ray diffraction study was carried out for investigating the crystalline structure of PVA/SnO_2/GO composite nanofibers before and after carbonization at different temperatures as depicted in Figure 6. A weak peak at 11.42°, related to (002) plane of GO, can be observed in the nanofibers of PVA/SnO_2/GO composite before carbonization. Also, there are the peaks at 19.68° and 22.48° which are assigned to the (101) and (200) planes of semi-crystalline PVA. The presence of the weak peaks at 26.61°, 33.86°, and 51.79°, related to the (110), (101), and (211) planes of SnO_2 respectively, suggests that the crystallization of rutile SnO_2 starts from the temperature of 400°C. Increasing the carbonization temperature causes the formation of crystalline SnO_2. The structural parameters of rutile tetragonal phase of SnO_2 were measured after carbonization at 650°C. Crystallite sizes of SnO_2 were calculated using the Scherrer formula: $D = 0.9\lambda/(\beta\cos\theta)$, where $\lambda = 1.5418$Å (Cu Kα), β = full width at half maximum, and θ = Bragg angle. Obtained results showed that crystallite sizes of SnO_2 were found to be 8.720nm, 6.270nm, and 7.614nm, respectively.

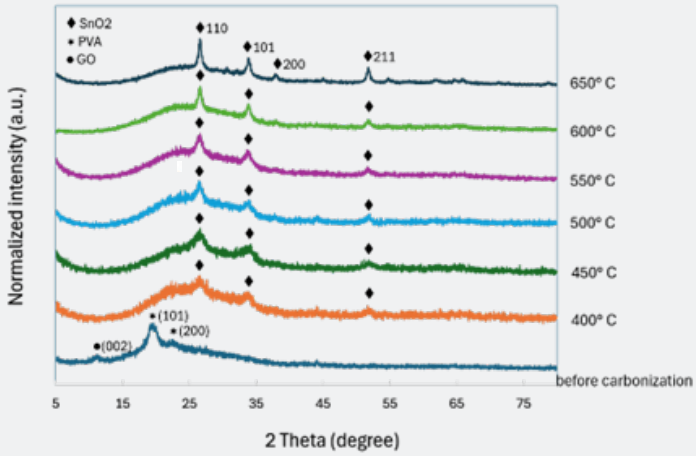

Figure 6: XRD spectrum of the composite nanofibers of PVA/SnO_2/GO before and after carbonization at different temperatures.

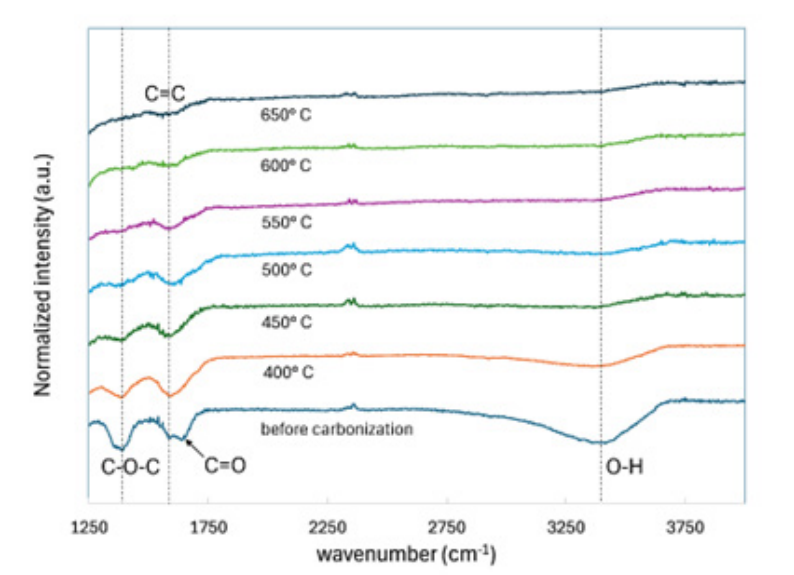

Figure 7: FTIR spectrum of the composite nanofibers of PVA/SnO_2/GO before and after carbonization at different temperatures.

How to cite this article: Chan W.Y., Lam K.C. Room-Temperature Methane Gas Sensing with Carbonization of Poly (Vinyl) Alcohol/Tin Dioxide/Graphene Oxide Nanofiber by Electrospinning. JOJ Material Sci. 2026; 10(4): 555792. DOI: 10.19080/JOJMS.2026.10.555792

FTIR analysis

The functional group analysis of the PVA/SnO_2/GO nanofibers using Fourier transform infrared (FTIR) spectroscopy before and after carbonization at various temperatures is shown in Figure 7. Prior to carbonization, strong peaks were observed for 1386cm^{-1} (C–O–C), 1587cm^{-1} (C=C), 1639cm^{-1} (C=O), and a wide peak was also observed for 3399cm^{-1} (O–H). These peaks indicated the presence of oxygen-containing functional groups including epoxy, carbonyl, hydroxyl, carboxylic, and aromatic groups on the surface of the PVA and GO within the nanofiber composite. As the carbonization temperature increased, the signal strength from the oxygen-containing groups gradually weakened and nearly completed pyrolysis was achieved at 650°C. In addition, compared with oxygen-containing functional groups, the aromatic C=C in GO revealed higher thermal stability since it took longer to decompose at 550°C.

Electrical measurement

The resistances of the PVA/SnO_2/GO composite nanofibers with different percentages of GO at various carbonization temperatures at ambient air were presented in Figure 8. Before carbonization, the composite nanofibers showed poor electrical conductivity at room temperature. With an increase in carbonization temperature, the resistance of the composite nanofibers decreased. PVA and GO act as p-type semiconductors with plenty of oxygen-containing functional groups which remove electrons from the materials to form a space charge region on the surface [80]. Hence, there is a decrease in surface conductivity. However, upon carbonization, the resistance of PVA and GO decreases as most oxygen functional groups are removed, making the composite materials less p-type. By adding SnO_2 to the composite PVA/GO materials, the resistance increases, attributed to the p-n junction effects at the surface between the p-type material and n-type SnO_2 [31,32]. The SnO_2 acts as an n-type semiconductor with many free electrons generated at the oxygen vacancies due to carbonization [11-13]. With an increase in the number of free electrons in SnO_2 transferred to the core of the PVA/GO material, there is a decrease in the number of free holes, hence increasing the resistance. However, the composite PVA/SnO_2/GO nanofibers remain p-type since oxygen present in the air occupies some oxygen vacancies in SnO_2 and transfers the free electrons to the surface. Therefore, there is more electron depletion at the core than the number of free holes from PVA and GO materials. The decrease in the resistance of the composite nanofibers with carbonization temperature could be attributed to two main reasons: (i) an increase in the removal of oxygen-containing functional groups in PVA and GO, and (ii) an increase in the number of oxygen vacancies in SnO_2, resulting from improved crystallinity of SnO_2 with increased carbonization temperatures [12]. This implies that there is increased electron transfer from the SnO_2 vacancies to the core, resulting in reduced composite nanofiber resistance. Generally, with an increase in the percentage of GO from 0 to 8wt%, there is a decrease in the resistance of the composite nanofibers.

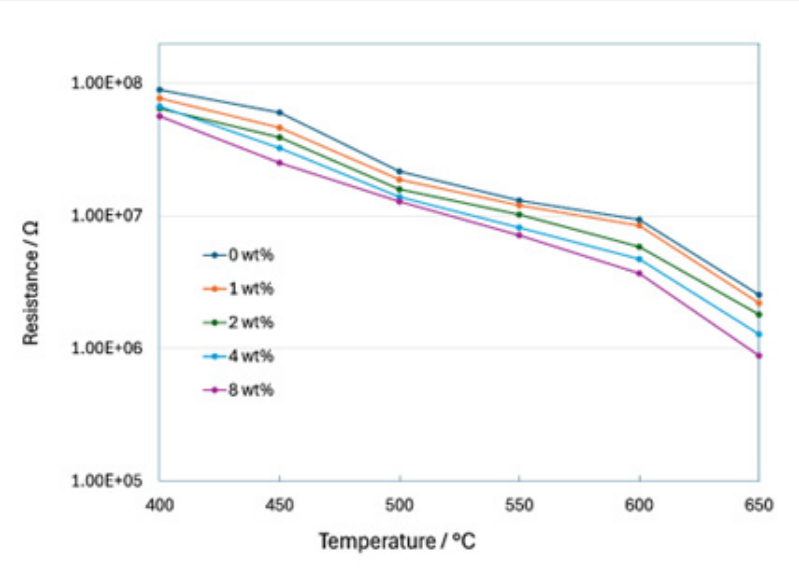

Figure 8: Resistances of the composite nanofibers PVA/SnO_2/GO with different GO contents carbonized at different temperatures.

Figure 9 presents the sensitivity of PVA/SnO_2/GO composite nanofibers with varied amounts of GO to methane (1%), measured at room temperature after carbonization at various temperatures. The sensitivity was calculated in a home-made gas chamber using the formula: (Rg – Ra)/Ra, where Rg is the resistance of the material sample in the presence of methane in ambient air, whereas Ra is the

How to cite this article: How to cite this article: Chan W.Y., Lam K.C. Room-Temperature Methane Gas Sensing with Carbonization of Poly (Vinyl) Alcohol/Tin Dioxide/Graphene Oxide Nanofiber by Electrospinning. JOJ Material Sci. 2026; 10(4): 555792. DOI: 10.19080/JOJMS.2026.10.555792

resistance after methane removal by ambient air. All samples were found to have positive sensitivity, which indicates the increase in resistance due to interaction with the reducing gas of methane with the p-type material sample. The sensitivity increased to a maximum value at 550°C carbonization temperature, beyond which there was a further decrease in the sensitivity at higher carbonization temperatures. Increased sensitivity between 400 to 550°C can be attributed to better crystallinity of SnO_2 that provides more oxygen vacancies for interaction with the gas [11-13]. Removal of oxygen-containing functional groups in PVA and GO had a smaller effect compared to crystallinity, considering that most of those functional groups could be removed around 400 to 450°C according to TGA and FTIR results. Sensitivities of the sensors dropped at higher temperatures than 550°C owing to reduced amounts of p-type amorphous carbon having oxygen functional groups that facilitate the p-n junction effect and sensitivity. This is supported by previous research indicating incomplete removal of oxygen groups even at 1100°C [33,81,82].

Sensitivity characteristics of PVA/SnO_2/GO composite nanofibers at different carbonization temperatures were noticed to be improved in the order of 0wt%, 1wt%, 2wt%, 4wt%, and 8wt%, as shown in Figure 9. As can be seen from this figure, the lowest sensitivity was obtained in the 0wt% composite nanofiber without GO. The low sensitivity might be due to the thin amorphous carbon layer around the SnO_2 layer as observed by TEM. In other words, the carbon layer prevented gases from reacting with SnO_2 layers and inhibited p-n junction effect due to reducing contact area between p-type amorphous carbon and n-type SnO_2 layers. In comparison, 1wt%–8wt% composite nanofibers with GO addition showed higher sensitivities than the 0wt% sample. The higher sensitivity could be caused by structural differences between composite nanofibers with and without GO. In detail, GO addition completely changed the core-shell structure to porous nanofiber structure, as observed by TEM. Porous nanofiber structure helped enhance gas-solid reactions and p-n junction effect through increasing the contact area between amorphous carbon and SnO_2. Sensitivity improved with an increase in GO percentage from 1wt% to 8wt%, owing to the enhanced formation of p-type amorphous carbon through carbonization, as analyzed by Raman spectroscopy and TGA test. The highest sensitivity of 8wt% could be resulted from the minimal amount of amorphous carbon covered on the nanofiber surface as PVA immobilization limits its diffusion after addition of GO [69-72].

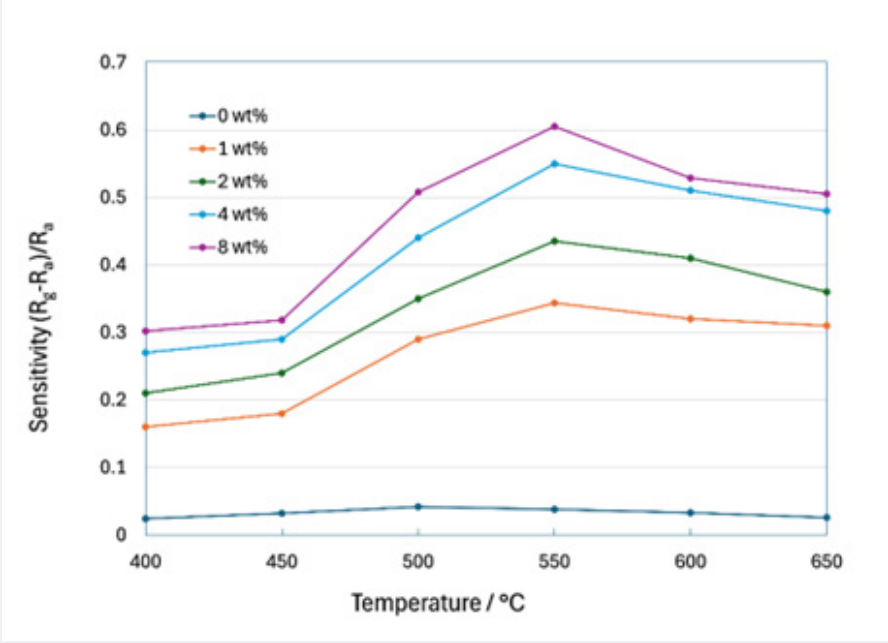

Figure 9: Sensitivities of the composite nanofibers PVA/SnO_2/GO with different GO contents carbonized at different temperatures towards methane (1%).

In Figure 10, sensitivities of PVA/SnO_2/GO composite nanofibers with different weight percentages of GO (i.e., 0wt%, 1wt%, 2wt%, 4wt%, and 8wt%) after carbonization at 550°C toward methane with different concentrations are given. For any weight percent, sensitivity increases as it becomes the largest when methane concentration reaches 10,000ppm. Among them, 8wt% sample gives the largest sensitivity of 60.5% at 10,000ppm. The gas sensor did not achieve saturation at concentration of 1,000–10,000ppm, which would be helpful in its practical application because most methane sensors tend to become saturated in this concentration range [48,83-86].

How to cite this article: Chan W.Y., Lam K.C. Room-Temperature Methane Gas Sensing with Carbonization of Poly (Vinyl) Alcohol/Tin Dioxide/Graphene Oxide Nanofiber by Electrospinning. JOJ Material Sci. 2026; 10(4): 555792. DOI: 10.19080/JOJMS.2026.10.555792

Table 1 shows an excellent summary of literature reports on room-temperature methane sensors compared to the current research work. It is vital to operate the methane gas sensor at room temperature since it helps significantly reduce the risk of explosions when operated at high temperatures [48–52]. It is worth noting that the PVA/SnO_2/GO nanofibers produced in this study exhibited electrical conductivity at room temperature with enhanced sensing response than other room-temperature methane sensors reported elsewhere. Moreover, the sensitivity of Pt-VO_2 became saturated at 1500ppm and started to decline [85], but the sensitivity of the PVA/SnO_2/GO nanofibers attained a value of 60.5% at 10,000ppm. In addition, the current manufacturing process used in this study is economically viable compared to other techniques that require decoration using expensive metals like palladium [87] and platinum [85]. Similarly, the preparation of carbon nanofibers obtained from polyvinyl alcohol is more economical than the carbon nanofibers derived from polyaniline [88-90] and polyacrylonitrile [57-60].

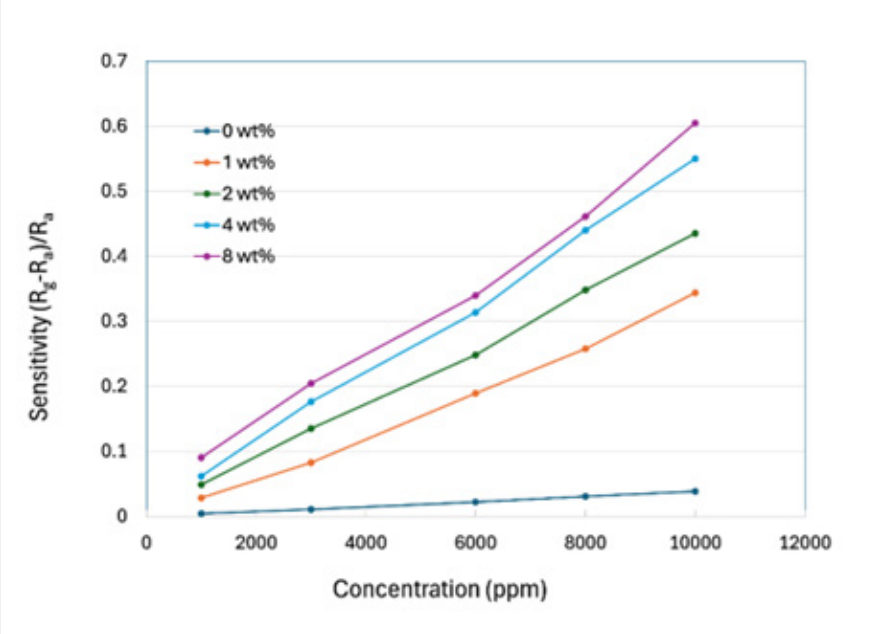

Figure 10: Sensitivities of the composite nanofiber with different GO contents after carbonization at 550°C towards methane at different concentrations.

Table 1: Recent reports on room temperature methane sensors.

Sensing Material	Technique	CH_4 Conc	Sensitivity	Refs
SnO_2 nanorods	Precipitation method	2,500ppm	0.58%	[91]
Graphene/PANI	Chemical method	3,200ppm	5%	[92]
VO_2	Pulsed dc sputtering	500ppm	3.2% (50 °C)	[93]
TiO2/n-Si	rf sputtering	1,000ppm	16% (50°C)	[94]
PbS nanocrystals	Chemical method	50,000ppm	47.60%	[95]
Pd doped SnO_2/RGO	Hydrothermal method	4,000ppm	2.07%	[87]
Pt-VO_2	dc-magnetron sputtering	1,500ppm	11.80%	[85]
$\alpha-Fe_{2-x}Cu_xO_3$	co-precipitation method	2,000ppm	5.70%	[96]
PVA/SnO_2/GO	Electrospinning method	1,000 – 10,000ppm	15.1 – 60.5 %	Present work

Conclusion

Resistance of PVA/SnO_2/GO composite nanofibers was successfully reduced via carbonization process with keeping sensitivity towards methane gas at room temperature in a high level. In the case of exposure to 10,000 ppm of methane gas, sensitivity was found as high as 60.5% at a carbonization temperature of 550°C and GO content of 8wt%. Due to the addition of GO to the composite nanofibers, the core-shell structure, which is formed without any addition of GO (at 0wt%), was successfully

How to cite this article: How to cite this article: Chan W.Y., Lam K.C. Room-Temperature Methane Gas Sensing with Carbonization of Poly (Vinyl) Alcohol/Tin Dioxide/Graphene Oxide Nanofiber by Electrospinning. JOJ Material Sci. 2026; 10(4): 555792. DOI: 10.19080/JOJMS.2026.10.555792

changed into a porous structure between 1wt% to 8wt%, thus improving sensitivity to methane gas considerably [91-94]. The porous structure of nanofibers significantly helps in increasing gas-solid interaction due to the increase of p-n junction effect and reducing shielding effects of the amorphous carbon layer. The developed room temperature gas sensor showed no saturation behavior between 1,000ppm to 10,000ppm of concentration range, suggesting that the proposed method can be used for higher concentration sensors.

Acknowledgement

The work described in this paper was partially supported by a grant from the College of Professional and Continuing Education, an affiliate of The Hong Kong Polytechnic University (Project No.: SEHS-2024-352(J)).

References

1. Arafat MM, Dinan B, Akbar SA, Haseeb ASMA (2012) Gas sensors based on one dimensional nanostructured metal-oxides: a review. Sensors 12(6): 7207-7208.
2. Huang J, Wan Q (2009) Gas sensors based on semiconducting metal oxide one-dimensional nanostructures. Sensors 9(12): 9903-9924.
3. Ding B, Wang M, Yu J, Sun G (2009) Gas sensors based on electrospun nanofibers. Sensors 9(3): 1609-1624.
4. Yang DJ, Kamienchick I, Youn DY, Rothschild A, Kim ID (2010) Ultrasensitive and highly selective gas sensors based on electrospun SnO_2 nanofibers modified by Pd loading. Adv Funct Mater 20(24): 4258-4264.
5. Choi JK, Hwang IS, Kim SJ, Park JS, Park SS, et al. (2010) Design of selective gas sensors using electrospun Pd-doped SnO_2 hollow nanofibers. Sensors and Actuators B: Chemical 150(1): 191-199.
6. Zhang Y, He X, Li J, Miao Z, Huang F (2008) Fabrication and ethanol-sensing properties of micro gas sensor based on electrospun SnO_2 nanofibers. Sens Actuators B Chem 132 (1): 67-73.
7. Watson J (1992) The tin oxide gas sensor and its applications. Sens Actuators 5(1): 29-42.
8. McAleer JF, Moseley PT, Norris JO, Williams DE (1987) Tin dioxide gas sensors. Part 1. -Aspects of the surface chemistry revealed by electrical conductance variations. J Chem Soc Faraday Trans 1 Phys Chem Condensed Phases 83(4): 1323-1346.
9. McAleer JF, Moseley PT, Norris JO, Williams DE, Tofield BC (1988) Tin dioxide gas sensors. Part 2. -The role of surface additives. J Chem Soc Faraday Trans 1 Phys Chem Condensed Phases 84(2): 441-457.
10. Ménini P, Parret F, Guerrero M, Soulantica K, Erades L, et al. (2004) CO response of a nanostructured SnO_2 gas sensor doped with palladium and platinum. Sens Actuators B Chem 103(1-2): 111-114.
11. Shen GL, Casanova R, Thornton G, Colera I (1991) Correlation between the surface conductivity and structure of SnO_2 (110). J Phys Condensed Matter 3: S291-S296.
12. Cox DF, Fryberger TB, Semancik S (1989) Surface reconstructions of oxygen deficient SnO_2 (110). Surf Sci 224(1-3): 121-142.
13. Oviedo J, Gillan MJ (2000) Energetics and structure of stoichiometric SnO_2 surfaces studied by first-principles calculations. Surf Sci 463(2): 93-101.
14. Horastani ZK, Sayedi SM, Sheikhi MH (2014) Effect of single wall carbon nanotube additive on electrical conductivity and methane sensitivity of SnO_2. Sens Actuators B Chem 202: 461-468.
15. Lee JH, Katoch A, Choi SW, Kim JH, Kim HW, et al. (2015) Extraordinary improvement of gas-sensing performances in SnO_2 nanofibers due to creation of local p–n heterojunctions by loading reduced graphene oxide nanosheets. ACS Appl Mater Interfaces 7(5): 3101-3109.
16. Lee JS, Kwon OS, Park SJ, Park EY, You SA (2011) Fabrication of ultrafine metal-oxide-decorated carbon nanofibers for DMMP sensor application. ACS Nano 5(10): 7992-8001.
17. Wang Z, Zhao C, Han T, Zhang Y, Liu S, et al. (2017) High-performance reduced graphene oxide-based room-temperature NO_2 sensors: A combined surface modification of SnO_2 nanoparticles and nitrogen doping approach. Sens Actuators B Chem 242: 269-279.
18. Wang Z, Li Z, Sun J, Zhang H, Wang W, et al. (2010) Improved hydrogen monitoring properties based on p-NiO/n-SnO_2 heterojunction composite nanofibers. J Phys Chem C 114(13): 6100-6105.
19. Yang A, Tao X, Wang R, Lee S, Surya C (2007) Room temperature gas sensing properties of SnO_2/multiwall-carbon-nanotube composite nanofibers. Appl Phys Lett 91(13): 133110.
20. Qi Q, Zhang T, Liu L, Zheng X (2009) Synthesis and toluene sensing properties of SnO_2 nanofibers. Sensors and actuators B: Chemical. Sens Actuators B Chem 137(2): 471-475.
21. Russo PA, Donato N, Leonardi SG, Baek S, Conte DE, et al. (2012) Room-temperature hydrogen sensing with hetero nanostructures based on reduced graphene oxide and tin oxide. Angew Chem Int Ed 51(44): 11053-11057.
22. Marichy C, Russo PA, Latino M, Tessonnier JP, Willinger MG, et al. (2013) Tin dioxide–carbon heterostructures applied to gas sensing: structure-dependent properties and general sensing mechanism. J Phys Chem C 117(38): 19729-19739.
23. Iski EV, Yitamben EN, Gao L, Guisinger NP (2013) Graphene at the Atomic-Scale: Synthesis, Characterization, and Modification. Adv Funct Mater 23(20): 2554-2564.
24. Allen MJ, Tung VC, Kaner RB (2010) Multi-scale approach for statistical broad absorption and emission spectra of organic compounds and biologic objects. Chem Rev 110: 132-145.
25. Wu S, He Q, Tan C, Wang Y, Zhang H (2013) Graphene-based electrochemical sensors. Small 9(8): 1160-1172.
26. Gan T, Hu S (2011) Electrochemical sensors based on graphene materials. Microchim Acta 175(1): 1-19.
27. Yuan W, Shi G (2013) Graphene-based gas sensors. J Mater Chem A 1(35): 10078-10091.
28. Chen D, Feng H, Li J (2012) Graphene oxide: preparation, functionalization and electrochemical applications. Chem Rev 112(11): 6027-6053.
29. Prezioso S, Perrozzi F, Giancaterini L, Cantalini C, Treossi E, et al. (2013) Graphene oxide as a practical solution to high sensitivity gas sensing. J Phys Chem C 117(20): 10683-10690.
30. Zhu Y, Murali S, Cai W, Li X, Suk JW, et al. (2010) Graphene and graphene oxide: synthesis, properties, and applications. Adv Mater 22(35): 3906-3924.
31. Mao S, Cui S, Lu G, Yu K, Wen Z, et al. (2012) Tuning gas-sensing properties of reduced graphene oxide using tin oxide nanocrystals. J Mater Chem 22(22): 11009-11013.
32. Lee JH, Katoch A, Choi SW, Kim JH, Kim HW, et al. (2015) Extraordinary improvement of gas-sensing performances in SnO_2 nanofibers due to creation of local p–n heterojunctions by loading reduced graphene oxide nanosheets. ACS Appl Mater Interfaces 7(5): 3101-3109.
33. Pei S, Cheng HM (2012) The reduction of graphene oxide. Carbon 50(9): 3210-3228.

How to cite this article: Chan W.Y., Lam K.C. Room-Temperature Methane Gas Sensing with Carbonization of Poly (Vinyl) Alcohol/Tin Dioxide/Graphene Oxide Nanofiber by Electrospinning. JOJ Material Sci. 2026; 10(4): 555792. DOI: 10.19080/JOJMS.2026.10.555792

34. Stankovich S, Dikin DA, Piner RD, Kohlhaas KA, Kleinhammes A, et al. (2007) Synthesis of graphene-based nanosheets via chemical reduction of exfoliated graphite oxide. Carbon 45(7): 1558-1565.

35. Merino MJF, Guardia L, Paredes JI, Rodil SV, Fernández PS, et al. (2010) Vitamin C as an innocuous and safe reductant for the preparation of graphene suspensions from graphite oxide. J Phys Chem C 114: 6426-6432.

36. Schniepp HC, Li JL, McAllister MJ, Sai H, Alonso MH, et al. (2006) Functionalized single graphene sheets derived from splitting graphite oxide. J Phys Chem B 110(17): 8535-8539.

37. Wang X, Zhi L, Müllen K (2008) Transparent, conductive graphene electrodes for dye-sensitized solar cells. Nano Lett 8(1): 323-327.

38. Mishra RK, Upadhyay SB, Kushwaha A, Kim TH, Murali G, et al. (2015) SnO_2 quantum dots decorated on RGO: A superior sensitive, selective and reproducible performance for a H_2 and LPG sensor. Nanoscale 7(28): 11971-11979.

39. Li D, Xia Y (2004) Electrospinning of nanofibers: reinventing the wheel. Adv Mater 16(14): 1151-1170.

40. Luo CJ, Stoyanov SD, Stride E, Pelan E, Edirisinghe M (2012) Electrospinning versus fiber production methods: from specifics to technological convergence. Chem Soc Rev 41(13): 4708-4735.

41. Doshi J, Reneker DH (1995) Electrospinning process and applications of electro spun fibers. Journal of electrostatics 35(2-3): 151-160.

42. Frenot A, Chronakis IS (2003) Polymer nanofibers assembled by electrospinning. Curr Opinion Colloid Interface Sci 8(1): 64-75.

43. Huang ZM, Zhang YZ, Kotaki M, Ramakrishna S (2003) A review on polymer nanofibers by electrospinning and their applications in nanocomposites. Compos Sci Technol 63(15): 2223-2253.

44. Anton F (1934) Process and apparatus for preparing artificial threads. US Patent No. 1,975,504.

45. Jirsak O, Sanetrnik F, Lukas D, Kotek V, Martinova L, et al. (2009) Method of nanofibers production from a polymer solution using electrostatic spinning and a device for carrying out the method. US Patent No. US7585437B2

46. Takahashi A, Urano Y, Tokuhashi K, Nagai H, Kaise M, et al. (1998) Fusing ignition of various metal wires for explosion limits measurement of methane/air mixture. Prev Process Ind 11(5): 353-360.

47. Min BK, Choi SD (2005) Undoped and 0.1 wt.% Ca-doped Pt-catalyzed SnO_2 sensors for CH_4 detection. Sensors and Actuators B: Chemical 108(1-2): 119-124.

48. Bhattacharyya P, Basu PK, Mondal B, Saha H (2008) A low power MEMS gas sensor based on nanocrystalline ZnO thin films for sensing methane. Microelectronics Reliability 48(11-12): 1772-1779.

49. Choudhary M, Mishra VN, Dwivedi R (2013) Solid-state reaction synthesized Pd-doped tin oxide thick film sensor for detection of H2, CO, LPG and CH4. J Mater Sci Mater Electron 24(8): 2824-2832.

50. Zhang D, Yin N, Xia B (2015) Facile fabrication of ZnO nanocrystalline-modified graphene hybrid nanocomposite toward methane gas sensing application. J Mater Sci Mater Electron 26(8): 5937-5945.

51. Zhang D, Chang H, Sun Y, Jiang C, Yao Y, et al. (2017) Fabrication of platinum-loaded cobalt oxide/molybdenum disulfide nanocomposite toward methane gas sensing at low temperature. Sens Actuators B Chem 252: 624-632.

52. Wang C, Li Y, Ding G, Xie X, Jiang M (2013) Preparation and characterization of graphene oxide/poly (vinyl alcohol) composite nanofibers via electrospinning. J Appl Polym Sci 127(4): 3026-3032.

53. Wang J, Wang X, Xu C, Zhang M, Shang X (2011) Preparation of graphene/poly (vinyl alcohol) nanocomposites with enhanced mechanical properties and water resistance. Polym Int 60(5): 816-822.

54. Zhang L, Wang Z, Xu C, Li Y, Gao J, et al. (2011) High strength graphene oxide/polyvinyl alcohol composite hydrogels. J Mater Chem 21(28): 10399-10406.

55. Yoo BM, Shin HJ, Yoon HW, Park HB (2014) Graphene and graphene oxide and their uses in barrier polymers. J Appl Polym Sci 131(1).

56. Zussman E, Chen X, Ding W, Calabri L, Dikin DA, et al. (2005) Mechanical and structural characterization of electrospun PAN-derived carbon nanofibers. Carbon 43(10): 2175-2185.

57. Lee KJ, Shiratori N, Lee GH, Miyawaki J, Mochida I, et al. (2010) Activated carbon nanofiber produced from electro spun polyacrylonitrile nanofiber as a highly efficient formaldehyde adsorbent. Carbon 48(15): 4248-4255.

58. Dong Q, Wang G, Qian B, Hu C, Wang Y, et al. (2014) Electro spun composites made of reduced graphene oxide and activated carbon nanofibers for capacitive deionization. Electrochimica Acta 137: 388-394.

59. Zhou Z, Lai C, Zhang L, Qian Y, Hou H, et al. (2009) Development of carbon nanofibers from aligned electro spun polyacrylonitrile nanofiber bundles and characterization of their microstructural, electrical, and mechanical properties. Polymer 50(13): 2999-3006.

60. Hummers WS, Offeman RE, (1958) Functionalized graphene and graphene oxide: Materials synthesis. Am J Chem Soc 80: 1339-1344.

61. Fong H, Chun I, Reneker DH (1999) Beaded nanofibers formed during electrospinning. Polymer 44(16): 4585-4592.

62. Lee KH, Kim HY, Bang HJ, Jung YH, Lee SG (2003) The change of bead morphology formed on electrospun polystyrene fibers. Polymer 44(14): 4029-4034.

63. Lin T, Wang H, Wang H, Wang X (2004) The charge effect of cationic surfactants on the elimination of fiber beads in the electrospinning of polystyrene. Nanotechnology 15(9): 1375-1381.

64. Deitzel JM, Kleinmeyer J, Harris DEA, Tan NB (2001) The effect of processing variables on the morphology of electrospun nanofibers and textiles. Polymer 42(1): 261-272.

65. Kong J, Liu Z, Yang Z, Tan HR, Xiong S, et al. (2012) Carbon/SnO_2/carbon core/shell/shell hybrid nanofibers: tailored nanostructure for the anode of lithium-ion batteries with high reversibility and rate capacity. Nanoscale 4(2): 525-530.

66. Xia X, Dong XJ, Wei QF, Cai YB, Lu KY (2012) Formation mechanism of porous hollow SnO_2 nanofibers prepared by one-step electrospinning. Express Polym Lett 6(2): 169-176.

67. Ji L, Rao M, Zheng H, Zhang L, Li Y, et al. (2011) Graphene oxide as a sulfur immobilizer in high performance lithium/sulfur cells. J Am Chem Soc 133(46): 18522-18525.

68. Pham TA, Choi BC, Jeong YT (2010) Facile covalent immobilization of cadmium sulfide quantum dots on graphene oxide nanosheets: preparation, characterization, and optical properties. Nanotechnology 21(46): 465603.

69. Sun S, Cao Y, Feng J, Wu P (2010) Click chemistry as a route for the immobilization of well-defined polystyrene onto graphene sheets. J Mater Chem 20(27): 5605-5607.

70. Chen X, Dai Y, Wang X, Guo J, Liu T, et al. (2015) Synthesis and characterization of Ag3PO4 immobilized with graphene oxide (GO) for enhanced photocatalytic activity and stability over 2, 4-dichlorophenol under visible light irradiation. J Hazard Mater 292: 9-18.

How to cite this article: How to cite this article: Chan W.Y., Lam K.C. Room-Temperature Methane Gas Sensing with Carbonization of Poly (Vinyl) Alcohol/Tin Dioxide/Graphene Oxide Nanofiber by Electrospinning. JOJ Material Sci. 2026; 10(4): 555792. DOI: 10.19080/JOJMS.2026.10.555792

71. Xu Y, Hong W, Bai H, Li C, Shi G (2009) Strong and ductile poly (vinyl alcohol)/graphene oxide composite films with a layered structure. Carbon 47(15): 3538-3543.

72. Yi M, Shen Z, Zhao X, Liu L, Liang S, et al. (2014) Exploring few-layer graphene and graphene oxide as fillers to enhance the oxygen-atom corrosion resistance of composites. Chem Phys 16(23): 11162-11167.

73. Tan Y, Song Y, Zheng Q (2012) Hydrogen bonding-driven rheological modulation of chemically reduced graphene oxide/poly (vinyl alcohol) suspensions and its application in electrospinning. Nanoscale 4(22): 6997-7005.

74. Wang B, Chen Z, Zhang J, Cao J, Wang S, et al. (2014) Fabrication of PVA/graphene oxide/TiO_2 composite nanofibers through electrospinning and interface sol–gel reaction: Effect of graphene oxide on PVA nanofibers and growth of TiO_2. Colloids Surf Physicochem Eng Asp 457: 318-325.

75. Tan P, Wen J, Hu Y, Tan X (2016) Adsorption of Cu^{2+} and Cd^{2+} from aqueous solution by novel electrospun poly (vinyl alcohol)/graphene oxide nanofibers. RSC Adv 6(83): 79641-79650.

76. Luo D, Zhang G, Liu J, Sun X (2011) Evaluation criteria for reduced graphene oxide. J Phys Chem C 115(23): 11327-11335.

77. Shen J, Hu Y, Shi M, Lu X, Qin C, et al. (2009) Fast and facile preparation of graphene oxide and reduced graphene oxide nanoplatelets. Chem Mater 21(15): 3514-3520.

78. Yamazoe N (1991) New approaches for improving semiconductor gas sensors. Sens Actuators B Chem 5(1-4): 7-19.

79. Mattevi C, Eda G, Agnoli S, Miller S, Mkhoyan KA, et al. (2009) Evolution of electrical, chemical, and structural properties of transparent and conducting chemically derived graphene thin films. Adv Funct Mater 19(16): 2577-2583.

80. Becerril HA, Mao J, Liu Z, Stoltenberg RM, Bao Z, et al. (2008) Evaluation of solution-processed reduced graphene oxide films as transparent conductors. ACS Nano 2(3): 463-470.

81. Basu PK, Jana SK, Saha H, Basu S (2008) Low temperature methane sensing by electrochemically grown and surface modified ZnO thin films. Sens Actuators B Chem 135(1): 81-88.

82. Penza M, Rossi R, Alvisi M, Suriano D, Serra E (2011) Pt-modified carbon nanotube networked layers for enhanced gas microsensors. Thin Solid Films 520(3): 959-965.

83. Liang J, Liu J, Li W, Hu M (2016) Preparation and room temperature methane sensing properties of platinum-decorated vanadium oxide films. Materials Research Bulletin 84: 332-339.

84. Horastani ZK, Sayedi SM, Sheikhi MH (2014) Effect of single wall carbon nanotube additive on electrical conductivity and methane sensitivity of SnO_2. Sens Actuators B Chem 202: 461-468.

85. Nasresfahani S, Sheikhi MH, Tohidi M, Zarifkar A (2016) Methane gas detection at room temperature using Pd doped SnO 2/reduced graphene oxide nanocomposite. 2016 24th Iranian Conference on Electrical Engineering (ICEE). IEEE.

86. Zhou S, Zhang H, Zhao Q, Wang X, Li J, et al. (2013) Graphene-wrapped polyaniline nanofibers as electrode materials for organic supercapacitors. Carbon 52: 440-450.

87. Gao Z, Yang W, Wang J, Yan H, Yao Y, et al. (2013) Electrochemical synthesis of layer-by-layer reduced graphene oxide sheets/polyaniline nanofibers composite and its electrochemical performance. Electrochimica Acta 91: 185-194.

88. Jianhua L, Junwei A, Yecheng Z, Yuxiao M, Mengliu L, et al. (2012) Preparation of an amide group-connected graphene–polyaniline nanofiber hybrid and its application in supercapacitors. ACS Appl Mater Interfaces 4(6): 2870-2876.

89. Labiosa AB, Solá F, Colón ML, Evans LJ, Xu JC, et al. (2012) A novel methane sensor based on porous SnO2 nanorods: room temperature to high temperature detection. Nanotechnology 23(45): 455501.

90. Wu Z, Chen X, Zhu S, Zhou Z, Yao Y, et al. (2013) Room temperature methane sensor based on graphene nanosheets/polyaniline nanocomposite thin film. IEEE Sens J 13(2): 777-782.

91. Prasad AK, Amirthapandian S, Dhara S, Dash S, Murali N, et al. (2014) Novel single phase vanadium dioxide nanostructured films for methane sensing near room temperature. Sens Actuators B Chem 191: 252-256.

92. Comert B, Akin N, Donmez M, Saglam S, Ozcelik S (2016) Titanium dioxide thin films as methane gas sensors. IEEE Sensors Journal 16(24): 8890-8896.

93. Mosahebfard A, Jahromi HD, Sheikhi MH (2016) Highly sensitive, room temperature methane gas sensor based on lead sulfide colloidal nanocrystals. IEEE Sensors Journal 16(11): 4174-4179.

94. Liu H, Peng T, Sun H, Xie R, Ma G (2017) Room temperature methane sensing properties of α-Fe_{2-x} Cu_xO_3 nanoparticles. RSC Adv 7(19): 11414-11419.

DOI: 10.19080/JOJMS.2026.10.555792

How to cite this article: Chan W.Y., Lam K.C. Room-Temperature Methane Gas Sensing with Carbonization of Poly (Vinyl) Alcohol/Tin Dioxide/Graphene Oxide Nanofiber by Electrospinning. JOJ Material Sci. 2026; 10(4): 555792. DOI: 10.19080/JOJMS.2026.10.555792